

CHANDRA HIGH-RESOLUTION SPECTRUM OF THE ANOMALOUS X-RAY PULSAR 4U 0142+61

ADRIENNE M. JUETT,¹ HERMAN L. MARSHALL, DEEPTO CHAKRABARTY,^{1,2} & NORBERT S. SCHULZ

Center for Space Research, Massachusetts Institute of Technology, Cambridge, MA 02139;

ajuett, hermann, deepto, nss@space.mit.edu

Accepted for publication in *ApJ Letters*

ABSTRACT

We report on a 25 ks observation of the 8.7 s anomalous X-ray pulsar 4U 0142+61 with the High Energy Transmission Grating Spectrometer (HETGS) on the *Chandra X-ray Observatory*. The continuum spectrum is consistent with previous measurements and is well fit by an absorbed power-law + blackbody with photon index $\Gamma = 3.3 \pm 0.4$ and $kT = 0.418 \pm 0.013$ keV. No evidence was found for emission or absorption lines, with an upper limit of ≈ 50 eV on the equivalent width of broad features in the 2.5–13 Å (0.95–5.0 keV) range and an upper limit of ≈ 10 eV on the equivalent width of narrow features in the 4.1–17.7 Å (0.7–3.0 keV) range. If the source is a magnetar, then the absence of a proton cyclotron line strongly constrains magnetar atmosphere models and hence the magnetic field strength of the neutron star. We find no strong features that are indicative of cyclotron absorption for magnetic field strengths of $(1.9\text{--}9.8) \times 10^{14}$ G. This is still consistent with the dipole field strength of $B = 1.3 \times 10^{14}$ G (at the polar cap) estimated from the pulsar's spindown.

Subject headings: pulsars: individual (4U 0142+061) — stars: neutron — X-rays: stars

1. INTRODUCTION

The anomalous X-ray pulsars (AXPs) have a number of properties that distinguish them as a class from other pulsars (Mereghetti & Stella 1995; van Paradijs, Taam, & van den Heuvel 1995). They have spin periods falling in a narrow range (6–12 s), luminosities of order $10^{34}\text{--}10^{35}$ erg s⁻¹, and a soft X-ray spectrum well described by a blackbody plus a power-law (see Gavriil & Kaspi 2002 and references therein). They also undergo relatively steady spin-down, have faint or unidentified optical counterparts, and show no evidence of binary motion. Several of the AXPs are associated with supernova remnants, indicating that they are relatively young neutron stars. Models to explain these properties fall into two general categories: accretion models and magnetar models.

In the accretion models, the accreting matter does not necessarily originate from a binary companion. X-ray timing and optical counterpart limits allow for only very low-mass companions, although it is difficult to reconcile such binaries with the supernova remnant associations because a supernova explosion would likely have unbound the binary. Another accretion model suggests that AXPs are isolated neutron stars accreting from a fallback disk of material from the supernova explosion or from the remains of a Thorne-Zytkow object (e.g., van Paradijs et al. 1995; Ghosh, Angelini, & White 1997). For all accretion models, there is an equilibrium pulsar spin period set by the mass accretion rate and the pulsar magnetic field strength. For the observed pulse periods and luminosities, the derived surface magnetic fields are of order 10^{11} G.

On the other hand, magnetar models have also been proposed, in which the AXPs are ultramagnetized ($B \sim 10^{14}\text{--}10^{15}$ G) neutron stars whose spin down is due to magnetic dipole radiation. In these models, the X-ray luminosity (which far exceeds the spin-down energy) arises from magnetic field interactions in the neutron star crust (see, e.g., Thompson & Duncan 1996). The spectral and timing properties of AXPs have been

used to constrain models for the atmospheres of ultramagnetized neutron stars (Özel, Psaltis, & Kaspi 2001). Other recent work on magnetar atmospheres has shown that proton cyclotron absorption features should be apparent in the soft X-ray spectrum of magnetars (Ho & Lai 2001; Zane et al. 2001). These lines are predicted to be broad ($\Delta E/E \approx 1$; Ho & Lai 2001). High-resolution soft X-ray spectroscopy should be able to test the magnetar model for AXPs.

The brightest known AXP is 4U 0142+61 ($l = 129^\circ 4$, $b = -0^\circ 4$), with a spin period of 8.7 s (see, Gavriil & Kaspi 2002, and references therein). Although long ago identified as an unusually soft X-ray source (Markert 1976; White & Marshall 1984; White et al. 1987), confusion with the nearby accretion-powered binary pulsar RX J0146.9+6121 contaminated the spectrum measured by early X-ray missions. More recent *ASCA* and *BeppoSAX* spectral studies measured a two component spectrum consisting of a 0.4 keV blackbody and a $\Gamma=3.7$ photon power-law (White et al. 1996; Israel et al. 1999; Paul et al. 2000). Hulleman, van Kerkwijk, & Kulkarni (2000) identified an optical counterpart based on the *Einstein* X-ray position, and 8.7 s optical pulsations have recently been reported (Kern & Martin 2001).

In this *Letter*, we discuss our *Chandra X-ray Observatory* High Energy Transmission Grating Spectrometer observation of 4U 0142+61. This is the first grating observation of an AXP obtained with *Chandra*. We show that the X-ray spectrum is consistent with previous lower resolution results and report on a search for line features in the spectrum. We place stringent limits on the strength of absorption lines and consequently the allowed magnetic field strengths assuming a magnetar model.

2. OBSERVATION AND DATA REDUCTION

We observed 4U 0142+61 with *Chandra* on 2001 May 23 for 25 ks using the High Energy Transmission Grating Spectrometer (HETGS) and the spectroscopy array of the Advanced CCD Imaging Spectrometer (ACIS-S). For a more detailed descrip-

¹ Also, Department of Physics, Massachusetts Institute of Technology

² Alfred P. Sloan Research Fellow

tion of the instruments, we defer to available *Chandra* X-ray Center (CXC) documents³. The HETGS employs two sets of transmission gratings: the Medium Energy Gratings (MEGs) with a range of 2.5–31 Å (0.4–5.0 keV) and the High Energy Gratings (HEGs) with a range of 1.2–15 Å (0.8–10.0 keV). The HETGS spectra were imaged by ACIS-S, an array of 6 CCD detectors. The HETGS/ACIS-S combination provides an undispersed (zerth order) image and dispersed spectra from the gratings. The various orders overlap and are sorted using the intrinsic energy resolution of the ACIS CCDs. The first-order HEG (MEG) spectrum has a resolution of $\Delta\lambda = 0.012$ Å (0.023 Å). The ACIS CCDs are normally read out every 3.2 s. In order to sample the 8.7-s pulse period of 4U 0142+61 more effectively, we designed the observation to read out only a 512-row subarray on the ACIS-S detectors, resulting in a frame time of only 1.8 s.

The “level 1” event file was processed using the CIAO v2.1 data analysis package⁴. During our analysis, it was found that the pipeline tool `acis_detect_afterglow` rejects 3–5% of source photons in grating spectra⁵. Afterglow is the residual charge left from a cosmic-ray event which is released over several frames and can cause a line-like feature in a grating spectrum; the tool attempts to identify afterglow by flagging events that occur at the same chip coordinates in consecutive frames. However, for bright sources like 4U 0142+61, the tool also rejects a small fraction of the valid source events. Although only a small fraction of the total, the rejection of source photons by this tool is systematic and non-uniform. Since order-sorting of grating spectra provides efficient rejection of background events, the afterglow detection tool is not necessary. Therefore, we reextracted the event file, retaining those events previously tagged by the `acis_detect_afterglow` tool in order to improve statistics. No spectral features were found that might be attributable to afterglow events.

The zeroth-order image of 4U 0142+61 was affected by photon pileup (see, e.g., Davis 2001b) and was not used in our spectral analysis. However, we used the zeroth-order image to measure the source position, with the CIAO tool `celldetect`. Our best-fit position was R.A.=01^h46^m22^s.44 and Dec.=61°45′03.″3 (equinox J2000.0), with an approximate error radius of 0.″5. The optical counterpart of Hulleman et al. (2000) lies 0.″46 from our X-ray position.

The combined MEG and HEG first order count rate was only 4.2 cts s⁻¹. We therefore did not expect the dispersed spectrum to be affected by pileup, although we made several checks nevertheless. First, the dispersion distance, d , of each event was compared to the energy determined by the intrinsic CCD resolution, E_{ACIS} . The grating equation predicts $E_{\text{ACIS}} = hc/\lambda = hcmR/(Pd)$, where R is the Rowland distance, m is the grating order, and P is the grating period. Sources with pileup show a deviation from this relationship in lower orders, as low order photons combine to produce higher energy events which are then attributed to higher orders. There were no signs of pileup from the observed dispersion-energy relationship. Also, separate model fits of the first and second order spectra were found to be consistent both with past (low-resolution) observations and with each other, with no signatures of pileup in the residuals. We conclude that pileup is negligible in our dispersed spectra.

We used the standard CIAO tools to create detector response files (ARFs; see Davis 2001a) for the MEG and HEG +1 and -1 order spectra. These were combined when the +/- order spectra were added for the HEG and MEG separately. The spectra were binned in two different ways. For continuum analysis, we binned the data at 0.08 Å with a minimum of 50 counts per bin. To look for high-resolution spectral features, the data were binned at 0.015 Å for the HEG and 0.03 Å for the MEG. We also created background files for the HEG and MEG spectra using the standard CIAO tools. Finally, we used the XSPEC v11 data analysis package (Arnaud 1996) to fit continuum models to the background-subtracted spectra.

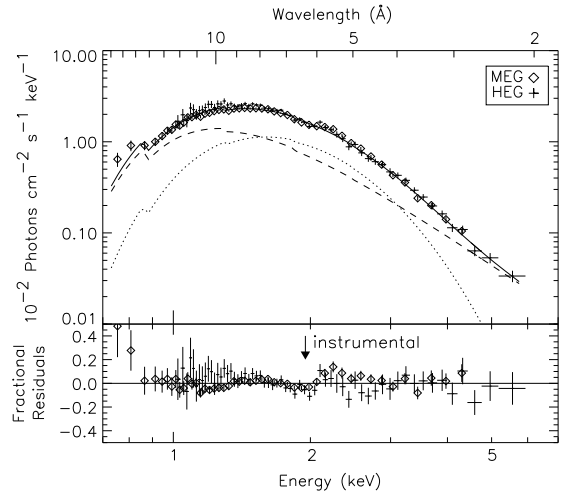


FIG. 1.— (upper panel) Unfolded MEG and HEG energy spectra of 4U 0142+61 fit with an absorbed power-law + blackbody model (solid line). The spectra have been coarsely binned for clarity. The contributions of the power-law (dashed line) and blackbody (dotted line) components are also shown. The normalization difference between the MEG and HEG is consistent with the uncertainty in the absolute flux calibration. (lower panel) Fractional residuals ($[\text{data} - \text{model}] / \text{model}$) from the absorbed power-law + blackbody model fit. The feature at ≈ 2 keV, marked with an arrow, is instrumental.

3. SEARCH FOR ABSORPTION FEATURES

We fit a variety of one and two component models to the coarsely binned HEG and MEG spectra: power-law, cutoff power-law, thermal bremsstrahlung, power-law + blackbody, power-law + disk blackbody, power-law + bremsstrahlung, bremsstrahlung + blackbody, and cutoff power-law + blackbody. All models included absorption by neutral interstellar gas with cosmic abundances. The *Chandra* best fit parameters of the most acceptable models are given in Table 1.

The cutoff power-law + blackbody best fit parameters were inconsistent and gave a cutoff energy far above the instrument bandpass, suggesting that a standard power-law model was sufficient. The one component models had larger reduced χ^2 values than the two component models and showed residuals that suggested the need for a second component. Using an F -test (see, e.g., Bevington & Robinson 1992), we determined that the addition of a blackbody to the power-law and bremsstrahlung models is highly significant. Therefore, we rule out the single component models: power-law, cutoff power-law, and thermal bremsstrahlung. The two component bremsstrahlung models all gave large emission measures $\approx 10^{58} d_{\text{kpc}}^2 \text{ cm}^{-3}$ which

³ <http://asc.harvard.edu/udocs/docs/docs.html>

⁴ <http://asc.harvard.edu/ciao/>

⁵ <http://asc.harvard.edu/ciao/threads/acisdetectafterglow/>

TABLE 1
CONTINUUM SPECTRAL FITS^a

Model ^b	N_{H} (10^{22} cm^{-2})	Γ or kT (or keV)	N^c	E_{cut} (keV)	kT_{bb} (keV)	R_{bb} (km)	χ^2/dof
PL	1.43 ± 0.03	4.02 ± 0.05	4.7 ± 0.2	515/259
PL + BB	0.88 ± 0.13	3.3 ± 0.4	1.0 ± 0.5	...	0.418 ± 0.013	2.0 ± 0.2	230/257
BREMS	0.92 ± 0.02	1.11 ± 0.02	1.13 ± 0.05	250/259
BREMS + BB	0.69 ± 0.07	1.6 ± 0.4	0.3 ± 0.2	...	0.391 ± 0.014	2.2 ± 0.3	227/257
CUTOFFPL	0.83 ± 0.06	0.9 ± 0.3	3.70 ± 0.19	0.93 ± 0.11	244/258

^aAll errors are quoted at the 90%-confidence level

^bPL: power-law, BB: blackbody, BREMS: bremsstrahlung, CUTOFFPL: cutoff power-law

^cPower-law normalization at 1 keV in units of $10^{-1} \text{ photons keV}^{-1} \text{ cm}^{-2} \text{ s}^{-1}$, bremsstrahlung normalization=emission measure in units of 10^{58} cm^{-3} .

would require an emission radius orders of magnitude larger than a neutron star for an optically thin plasma (White et al. 1996), and were rejected on this basis. Traditionally, the source has been fit with an absorbed power-law + blackbody model and our analysis favors this model as well. The results of the *Chandra* fit, summarized in Table 1 and shown in Figure 1, are consistent with previous observations of 4U 0142+61. When the same model is applied to the high-resolution binned data set, the same parameter values are found to within the uncertainties.

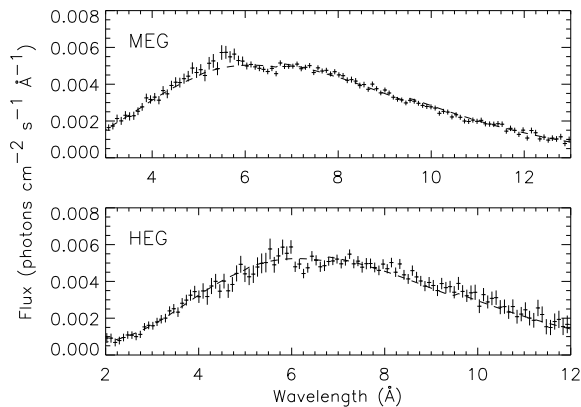


FIG. 2.— MEG and HEG spectra of 4U 0142+61 at 6 \times and 12 \times instrument resolution, respectively. The best fit absorbed power-law + blackbody model is shown as a dashed line. The misfit of the continuum between 5.5–7.0 \AA is not consistent in the MEG and HEG spectra, and is attributed to instrumental features around known absorption edges. The spectra show no deep features that might result from proton cyclotron resonance absorption in a magnetic field in the range of $(1.9\text{--}9.8) \times 10^{14} \text{ G}$.

With this continuum model, we then looked for absorption and emission features in the high-resolution spectrum. We searched for both narrow and broad line-like features. An initial inspection of the residuals of the power-law + blackbody model fit seemed to show a feature at $\approx 6 \text{ \AA}$ (2 keV; see Figure 1). This feature is however highly suspect, since it is located between two known instrumental edges (Si-K at 6.75 \AA and Ir-M at 5.98 \AA). It does not appear in the MEG +1 spectrum (which is on a back-illuminated chip) but only in the MEG –1 and HEG +1/–1 spectra (on front-illuminated chips). Furthermore, the dip occurs at a slightly different energy and with a

different depth in the MEG and HEG spectra (see Figure 2). For these reasons, we conclude that the feature is instrumental.

To search for broad features, we used the high-resolution HETGS spectra and fit Gaussian line models to the fractional residuals ($[\text{data-model}]/\text{model}$) of the continuum fit. The central energies and widths of the Gaussian components were fixed, while the normalizations were fitted. To look for features that had been predicted in the magnetar models (Ho & Lai 2001; Zane et al. 2001), the sigma of the Gaussian was chosen to vary with energy ($\sigma = 0.1 \times E$). The Gaussian model was fit to the data centering at every wavelength point. We were able to determine the best fit amplitude and standard deviation of this result as well as the significance of each feature. The 4σ upper limits on the equivalent widths (EWs) of any features are shown in Figure 3. There were no features with a significance greater than 4σ , which we believe is a reasonable lower limit. In Figure 3, we have also included lines which mark the equivalent width limits for $\text{EW}=0.1E$ and $\text{EW}=0.5E$ for comparison.

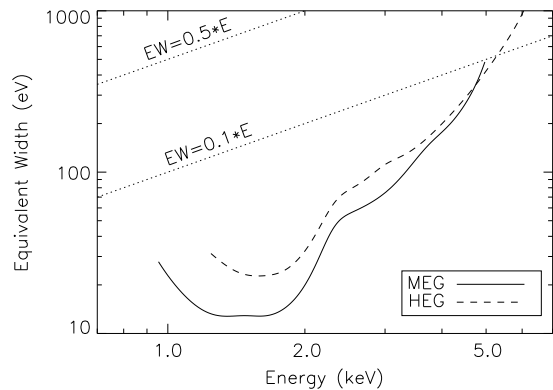


FIG. 3.— Upper bounds on the equivalent widths of lines with intrinsic width $\sigma = 0.1E$ (where E is the line energy). Magnetar atmosphere models predict that the equivalent width of a proton cyclotron absorption line is of order $0.70\text{--}0.75E$ (Zane et al. 2001), although more recent work predicts equivalent widths at least an order of magnitude lower (Ho & Lai 2002). For comparison, we have included lines which define $\text{EW}=0.5E$ and $\text{EW}=0.1E$. We conclude that the spectra show no strong absorption feature attributable to the proton cyclotron resonance in a magnetic field in the range of $(1.9\text{--}9.8) \times 10^{14} \text{ G}$.

Similarly, no narrow line features were found in the high-resolution spectra. We can place a 3σ upper limit of 10 eV on any emission line between 4.1–17.7 \AA (0.7–3.0 keV) whose width (FWHM) is comparable to the instrument resolution (see

Figure 4). The computation uses the model fit to the time-averaged HEG and MEG data. We assume that candidate features are only 2 bins wide. One may derive limits on broader features until the scale of the feature becomes comparable to that of the instrument calibration uncertainties. Limits on absorption lines are identical when there are $\gtrsim 25$ counts per bin but are systematically larger for $\lesssim 25$ counts per bin.

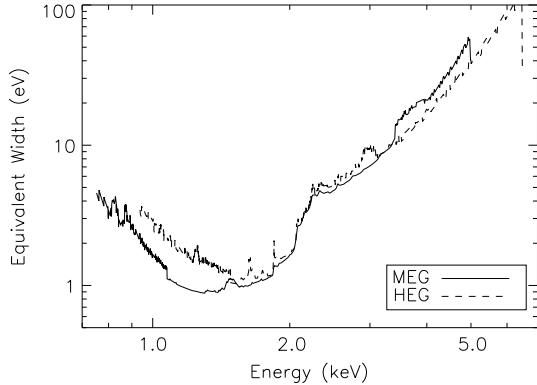


FIG. 4.— Upper bounds on the equivalent widths of narrow lines with FWHMs comparable to the instrument resolution, 0.023 \AA (0.012 \AA), for MEG (HEG). We assumed that candidate features are only 2 bins wide. One may derive limits on broad features using these curves until the scale of the feature becomes comparable to that of the instrument calibration uncertainties. Limits on absorption lines are identical when there are $\gtrsim 25$ counts per bin but are systematically larger for $\lesssim 25$ counts per bin.

4. DISCUSSION

The *Chandra* spectrum of 4U 0142+61 is well fit by an absorbed power-law + blackbody, which is consistent with previous observations of the source (White et al. 1996; Israel et al. 1999; Paul et al. 2000). The small radius of the blackbody model might be explained by atmospheric effects which give an overestimation of the temperature and thus an underestimation of the radius when fit by a standard blackbody (see, e.g., Perna et al. 2001, and references therein). The best fit hydrogen column density of $(0.88 \pm 0.13) \times 10^{21} \text{ cm}^{-2}$ is consistent with estimates derived from radio and optical studies (Dickey & Lockman 1990; Hulleman et al. 2000). Distance estimates from extinction measurements for 4U 0142+61 range from 1–5 kpc due to the line of sight passing through the edge of a local (< 1 kpc) molecular cloud. When including effects of the molecular cloud, a lower limit of 1 kpc is determined, whereas when neglecting the molecular cloud a lower limit of 2.7 kpc is obtained (Özel et al. 2001). Normalizing the distance to 1 kpc,

we find a luminosity (0.5–10 keV) of $5.3 \times 10^{34} d_{\text{kpc}}^2 \text{ ergs s}^{-1}$ which is consistent with past measurements from *ASCA* and *BeppoSAX*.

No significant discrete features were found in the high-resolution spectrum. We can place a limit on the equivalent width of any narrow feature of $\approx 10 \text{ eV}$ in the range $4.1\text{--}17.7 \text{ \AA}$ (0.7–3.0 keV) and $\approx 50 \text{ eV}$ for broad features in the range $2.5\text{--}13 \text{ \AA}$ (0.95–5.0 keV). The limits on the equivalent width of any absorption features place strong constraints on the neutron star atmosphere models. Atmosphere models of ultramagnetized neutron stars predict a broad proton cyclotron absorption feature at an energy $E_B = 0.63 y_g (B/10^{14} \text{ G}) \text{ keV}$, where $y_g = (1 - 2GM/c^2R)^{1/2}$ is the gravitational redshift factor and B is the surface magnetic field strength (Ho & Lai 2001; Zane et al. 2001). If we assume that magnetic dipole radiation drives the spindown, the magnetic field strength found using P and \dot{P} ($B^2 \propto P\dot{P}$) is $1.3 \times 10^{14} \text{ G}$ (Gavriil & Kaspi 2002). A dipole field produces a cyclotron absorption feature consistent with a surface magnetic field strength 20–30% lower (Zane et al. 2001). For 4U 0142+61, the dipole field of $1.3 \times 10^{14} \text{ G}$ would give a cyclotron absorption feature at $\approx 0.5 \text{ keV}$, which is well outside of the range accessible to our observation.

Initial theoretical work predicted a proton cyclotron absorption feature of equivalent width $0.70\text{--}0.75 E_B$ (Ho & Lai 2001; Zane et al. 2001), which is much greater than the equivalent width limits in the 0.95–5.0 keV range. If we take $y_g \sim 0.8$, the above energy range corresponds to magnetic field strengths of $(1.9\text{--}9.8) \times 10^{14} \text{ G}$. More recent work has shown that vacuum polarization effects strongly suppress the cyclotron absorption feature, giving equivalent widths an order of magnitude lower (Ho & Lai 2002). It should also be noted that the theoretical calculations of the equivalent width of the cyclotron feature were done for a local patch of the neutron star surface. A phase averaged spectrum, like the one we are using, would include contributions from various magnetic field strengths, directions and effective temperatures, which would further suppress the cyclotron feature. The combination of these effects may reduce the predicted equivalent widths to below our measured values for much of the spectral range we studied.

We thank Claude R. Canizares, the HETGS principal investigator, for allocating part of his *Chandra* guaranteed time program to this observation. We also thank Wynn C. G. Ho, Dong Lai, Feryal Özel, Dimitrios Psaltis, and Peter Woods for useful discussions. This research was supported in part by contracts SAO SV1-61010 and NAS8-38249 as well as NASA grant NAG5-9184.

REFERENCES

- Arnaud, K. A. 1996, in *Astronomical Data Analysis Software and Systems V*, ed. G. Jacoby & J. Barnes (San Francisco: ASP Conf. Ser. 101), 17
- Bevington, P. R., & Robinson, D. K. 1992, *Data Reduction and Error Analysis for the Physical Sciences*, 2nd ed. (New York: McGraw-Hill)
- Davis, J. E. 2001a, *ApJ*, 548, 1010
- . 2001b, *ApJ*, 562, 575
- Dickey, J. M., & Lockman, F. J. 1990, *Ann. Rev. Ast. Astr.*, 28, 215
- Gavriil, F. P., & Kaspi, V. M. 2002, *ApJ*, in press (astro-ph/0107422)
- Ghosh, P., Angelini, L., & White, N. E. 1997, *ApJ*, 478, 713
- Ho, W. C. G., & Lai, D. 2001, *MNRAS*, 327, 1081
- Ho, W. C. G., & Lai, D. 2001, *MNRAS*, submitted (astro-ph/0201380)
- Hulleman, F., van Kerkwijk, M. H., & Kulkarni, S. R. 2000, *Nature*, 408, 689
- Israel, G. L. et al. 1999, *A&A*, 346, 929
- Kern, B., & Martin, C. 2001, *IAU Circ.*, No. 7769
- Markert, T. H. 1976, PhD thesis, Massachusetts Institute of Technology
- Mereghetti, S., & Stella, L. 1995, *ApJ*, 442, L17
- Özel, F. 2001, *ApJ*, 563, 276
- Özel, F., Psaltis, D., & Kaspi, V. M. 2001, *ApJ*, 563, 255
- Paul, B., Kawasaki, M., Dotani, T., & Nagase, F. 2000, *ApJ*, 537, 319
- Perna, R., Heyl, J. S., Hernquist, L. E., Juett, A. M., & Chakrabarty, D. 2001, *ApJ*, 557, 18
- Thompson, C., & Duncan, R. C. 1996, *ApJ*, 473, 322
- Thorne, K. S., & Zytow, A. N. 1977, *ApJ*, 212, 832
- van Paradijs, J., Taam, R. E., & van den Heuvel, E. P. J. 1995, *A&A*, 299, L41
- White, N. E., Angelini, L., Ebisawa, K., Tanaka, Y., & Ghosh, P. 1996, *ApJ*, 463, L83
- White, N. E., & Marshall, F. E. 1984, *ApJ*, 281, 354
- White, N. E., et al. 1987, *MNRAS*, 226, 645
- Zane, S., Turolla, R., Stella, L., & Treves, A. 2001, *ApJ*, 560, 384